

Large eddy simulations of the flow around a circular cylinder: effects of grid resolution and subgrid scale modeling

E. Salvatici[†] and M.V. Salvetti[‡]

Dipartimento di Ingegneria Aerospaziale, Università di Pisa, V. G. Caruso, 56122 Pisa, Italy

(Received November 30, 2002, Accepted August 6, 2003)

Abstract. Large-eddy simulations of the flow around a circular cylinder at a Reynolds number, based on cylinder diameter and free-stream velocity, $Re_D=2\times 10^4$ are presented. Three different dynamic subgrid-scale models are used, viz. the dynamic eddy-viscosity model and two different mixed two-parameter models. The sensitivity to grid refinement in the spanwise and radial directions is systematically investigated. For the highest resolution considered, the effects of subgrid-scale modeling are also discussed in detail. In particular, it is shown that SGS modeling has a significant influence on the low-frequency modulations of the aerodynamics loads, which are related to significant changes in the near wake structure.

Keywords: large eddy simulation; subgrid scale modeling; grid resolution.

1. Introduction

As flows of engineering or industrial interest are usually characterized by high Reynolds numbers, a turbulence model is needed in numerical simulations. It is known that statistical turbulence models, such as those used in the RANS approach, usually have difficulties in accurately predicting the flow around bluff bodies. Conversely, since large-scale eddy structures dominate the turbulent transport, and unsteady processes like vortex shedding are the prevailing features, large-eddy simulation (LES), in which the largest scales of the flow are explicitly resolved, seems to be particularly well suited. However, although in the last decade LES has increasingly been applied to the simulation of bluff body flows, a few problems remain to be solved before LES may become a completely reliable tool for the prediction of quantities of practical interest, such as the aerodynamic loads. In particular, the level of numerical resolution (i.e., accuracy of the scheme and grid refinement) needed to obtain accurate results is far from being established. Furthermore, it is not clear whether and how this depends on the physical modeling of the small scales (SGS modeling).

Among bluff-body flows, the flow around a circular cylinder is certainly one of the most challenging test cases from a numerical point of view. Recently, a few examples of large-eddy simulations of the flow around circular cylinders have appeared in the literature (Mittal and Moin

[†] PhD. Student

[‡] Associate Professor

1997, Breuer 1998, Fröhlich, *et al.* 1998, Jordan and Ragab 1998, Breuer 2000, Kravchenko and Moin, 2000, Ma, *et al.* 2000, Lübecke, *et al.* 2001, Franke and Frank 2002). Most of these LES are at low Reynolds numbers, of the order of 10^3 based on the free-stream velocity and the cylinder diameter D . From these studies it arises that highly resolved grids are needed to obtain reliable results. For instance, the conclusion of Kravchenko and Moin (2000) was that “simulations over a cylinder require grids that take all essential flow scales into consideration to accurately reproduce the near-wake flow statistics”. In spite of this high level of resolution, significant discrepancies were observed between the different computations, especially in the near wake (recirculation length, shape of the mean streamwise velocity profiles). Ma, *et al.* (2000) attributed the aforementioned differences to the spanwise extent of the computational domain and to the background fluctuations level. Indeed, they showed that the near wake structure significantly changes with these parameters. Franke and Frank (2002) suggested that the discrepancies could also be due to different averaging times. In particular, they found that extremely long times are needed to obtain converged mean values. Finally, the different LES were in disagreement also on the effect of the subgrid scale model. Indeed, Ma, *et al.* (2000) found that the near wake structure changes significantly by increasing the subgrid scale viscosity. Conversely, in Kravchenko and Moin (2000) and Breuer (1998) the influence of the SGS model was found to be insignificant, as expected in those low Reynolds and highly resolved simulations.

Clearly, if LES is to be used as a predictive tool for practical applications, and thus for significantly higher Reynolds numbers, only a much coarser resolution can be achieved due to computer limitations, and, thus, the SGS modeling is expected to play a more fundamental role. A recent example of LES of the flow past a circular cylinder at a higher Reynolds number ($Re_D = 1.4 \times 10^5$) can be found in Breuer (2000). In that study, the SGS model was found to have a significant influence but the superiority of a particular model among those considered could not be proved. Moreover, an astonishing outcome was that grid refinement did not automatically lead to improved results for all quantities. A second LES at $Re_D = 1.4 \times 10^5$ is briefly presented in Lübecke, *et al.* (2001); however, the results are quite far from those in Breuer (2000) and from experiments (Cantwell and Coles 1983), probably due to the much coarser grid that was used.

Thus, in our opinion, particularly for LES of the flow around circular cylinders we are far from having established the numerical resolution required to have a satisfactory prediction of at least the most significant parameters for engineering applications. In addition, it is not clear how and whether this depends on SGS modeling.

The main goal of the present work is to give a contribution to this problem. To this aim, a Reynolds number of 2×10^4 has been chosen, which is still in the sub-critical regime, but is one order of magnitude larger than the values used in the low-Reynolds LES in the literature, and we started from a much coarser grid resolution than in those LES. Besides the classical dynamic eddy-viscosity model (DSM) (Germano, *et al.* 1991), a two-parameter dynamic mixed model (DTM) (Salvetti and Banerjee 1995) is also employed. In previous a priori tests and large-eddy simulations, mixed models have been found to give significant improvements with respect to eddy-viscosity models (see, for instance, Meneveau and Katz 2000). Note, however, that in the previous LES of circular cylinder flows in the literature only eddy-viscosity models have been used. In Salvetti and Beux (2000) we carried out some preliminary simulations of the flow around a circular cylinder at $Re_D = 2 \times 10^4$, investigated experimentally in Yokuda and Ramaprian (1990), with very coarse grid resolution. As expected, the effects of SGS modeling were found to be significant and a better global agreement with experiments was found with the DTM. However, significant discrepancies

with experiments were present in the separated wake for both models. On the basis of these results, in the present work we carry out a further analysis by progressively refining the grid in the spanwise direction, with the DSM and the DTM. Simulations on a grid further refined in the radial direction are also presented for the DSM, the DTM and a recently proposed modified version of the DTM (Morinishi and Vasilyev 2001), which is expected to have a better behavior near solid walls. In particular, the effects of SGS modeling on the near wake structure and on low-frequency modulations of the aerodynamic loads are investigated.

2. Mathematical formulation and numerical method

The continuity and momentum equations for incompressible flows with constant properties are considered. When a filter is applied, the effects of the unresolved subgrid scales appear in the Navier-Stokes equations:

$$\frac{\partial \bar{u}_i}{\partial t} + \bar{u}_j \frac{\partial \bar{u}_i}{\partial x_j} = -\frac{1}{\rho} \frac{\partial \bar{p}}{\partial x_i} + 2\nu \frac{\partial \bar{S}_{ij}}{\partial x_j} - \frac{\partial \tau_{ij}}{\partial x_j} \quad (1)$$

in which u_i is the velocity component in the i direction, the overbar denotes the filtering operation, \bar{S}_{ij} is the filtered strain rate tensor:

$$\bar{S}_{ij} = \frac{1}{2} \left(\frac{\partial \bar{u}_i}{\partial x_j} + \frac{\partial \bar{u}_j}{\partial x_i} \right) \quad (2)$$

and

$$\tau_{ij} = \bar{u}_i \bar{u}_j - \bar{u}_i \bar{u}_j \quad (3)$$

is the subgrid scale stress tensor, which expresses the effect of scales smaller than the filter width. This term has to be modeled to close the problem.

Several SGS models have been proposed in the literature. If attention is focussed on eddy-viscosity and mixed models, the following general form may be used:

$$\tau_{ij} - \frac{\delta_{ij}}{3} \tau_{kk} = -2C\bar{\Delta}^2 |\bar{S}| \bar{S}_{ij} + K \left(L_{ij}^m - \frac{\delta_{ij}}{3} L_{kk}^m \right) \quad (4)$$

where $\bar{\Delta}$ is the filter width, $|\bar{S}| = (2\bar{S}_{ij} \bar{S}_{ij})^{1/2}$, C and K are the unknown coefficients of the model and

$$L_{ij}^m = \bar{u}_i \bar{u}_j - \bar{u}_i \bar{u}_j \quad (5)$$

is the modified Leonard term.

The most widely used SGS model in early LES is due to Smagorinsky (1963) and can be obtained from Eq. (1) by setting $K=0$ and by considering C as a constant, which must be specified *a priori*. This model has some drawbacks: the input model parameter C is in fact flow and time

dependent, an incorrect limiting behavior near solid walls and in laminar flow is obtained ($\tau_{ij}=0$ only if $\widehat{S}_{ij}=0$), and it is impossible to account for the backscatter of energy from small scales to large scales, since the model is always dissipative ($C>0$).

The dynamic subgrid stress model (DSM) proposed by Germano, *et al.* (1991) overcomes most of the limitations of the Smagorinsky model. It employs the eddy-viscosity Smagorinsky expression of τ_{ij} , but the unknown coefficient C is directly computed following the dynamic procedure proposed in Germano, *et al.* (1991). In this way, the model coefficient C is obtained as a function of space and time, and no input parameter is required. Furthermore, the DSM has the correct asymptotic behavior near a wall and in laminar flow and permits energy backscatter from small scales to large scales, because negative values of C are also allowed. Nevertheless, the DSM still has some aspects to be improved, because the assumption that τ_{ij} is proportional S_{ij} is not generally correct. From a practical viewpoint, the most serious problem in LES computations with the DSM is, however, the presence of large fluctuations of the model coefficient, arising when it is computed locally, which often leads to numerical instability.

Zang, *et al.* (1993) proposed a dynamic mixed model (DMM) using an extension (the modified Leonard term) of the Bardina scale-similarity model (Bardina, *et al.* 1984). The model coefficient C is computed as a function of time and space following the same dynamic procedure used for the DSM and K is a constant set equal to 1. Salvetti and Banerjee (1995) improved upon that model and defined a dynamic two-parameter model (DTM). They showed that both coefficients C and K could be computed with a dynamic procedure. The DMM, and in a larger extent the DTM, have shown a better correlation with exact SGS stresses and energy than the DSM in a priori tests with filters in physical space. The behavior of the eddy-viscosity coefficient C is also significantly improved.

We now describe the dynamic procedure for computing the coefficients of the previously cited dynamic models. A test filter (denoted by $\widehat{\cdot}$), which has larger width than the grid filter, is applied to (1). In the double-filtered Navier-Stokes equations the subtest strain tensor T_{ij} appears:

$$T_{ij} = \widehat{\widehat{u_i u_j}} - \widehat{\widehat{u_i}} \widehat{\widehat{u_j}} \quad (6)$$

which is modeled analogously to τ_{ij} :

$$T_{ij} - \frac{\delta_{ij}}{3} T_{kk} = -2C \widehat{\Delta}^2 |\widehat{S}| \widehat{S}_{ij} + K \left(L_{ij}^t - \frac{\delta_{ij}}{3} L_{kk}^t \right) \quad (7)$$

where $\widehat{\Delta}$ is the dimension of the test filter and

$$L_{ij}^t = \widehat{\widehat{u_i u_j}} - \widehat{\widehat{u_i}} \widehat{\widehat{u_j}} \quad (8)$$

The following algebraic identity was demonstrated by Germano *et al.* (1991):

$$D_{ij} = \widehat{\widehat{u_i u_j}} - \widehat{\widehat{u_i}} \widehat{\widehat{u_j}} = T_{ij} - \widehat{\tau_{ij}} \quad (9)$$

By introducing Eqs. (4) and (7) in Eq. (9), the following tensorial equation is obtained:

$$D_{ij}^* = -2C\bar{\Delta}^2 M_{ij} + KH_{ij}^* \quad (10)$$

where:

$$M_{ij} = \frac{\hat{\Delta}^2}{\Delta^2} |\hat{S}| \hat{S}_{ij} - |\widehat{S}| \widehat{S}_{ij} \quad (11)$$

$$H_{ij} = \widehat{\widehat{u}_i \widehat{u}_j} - \widehat{\widehat{u}_i} \widehat{\widehat{u}_j} \quad (12)$$

and the asterisk indicates the deviatoric part of each tensor. To compute C and K , a technique of square error minimization is used, i.e., let Q be the square of the error in Eq. (10):

$$Q = (D_{ij}^* + 2C\bar{\Delta}^2 M_{ij} - KH_{ij}^*)^2 \quad (13)$$

the values of the two coefficients are obtained by imposing $\partial Q/\partial C = 0$ and $\partial Q/\partial K = 0$.

This leads to the following linear system:

$$\underbrace{\begin{pmatrix} H_{ij}^* H_{ij}^* & -2\bar{\Delta}^2 H_{ij}^* M_{ij} \\ -2\bar{\Delta}^2 H_{ij}^* M_{ij} & 4\bar{\Delta}^4 M_{ij} M_{ij} \end{pmatrix}}_A \begin{pmatrix} K \\ C \end{pmatrix} = \begin{pmatrix} D_{ij}^* H_{ij}^* \\ -2\bar{\Delta}^2 D_{ij}^* M_{ij} \end{pmatrix} \quad (14)$$

For the DTM we obtain:

$$K = \frac{-(D_{ij}^* H_{ij}^*)(M_{ij} M_{ij}) + (D_{ij}^* M_{ij})(H_{ij}^* M_{ij})}{(H_{ij}^* M_{ij})^2 - (H_{ij}^*)^2 (M_{ij} M_{ij})} \quad (15)$$

and

$$C = \frac{H_{ij}^* M_{ij} K - D_{ij}^* M_{ij}}{2\bar{\Delta}^2 M_{ij} M_{ij}} \quad (16)$$

The value of C for the DMM and the DSM can be obtained from Eq. (16), by setting $K=1$ and $K=0$ respectively.

Recently, Morinishi and Vasilyev (2001) have proposed a modification of the DTM (DTMR) that differs from this one for the dynamic computation of the unknown coefficients. Starting from the observation that the condition number of the matrix A is large, especially near solid walls, they introduce an approximation of A . In particular, since $|A_{21}| \ll |A_{22}|$ near the wall, A is approximated

by the triangular matrix:

$$\begin{pmatrix} A_{11} & A_{12} \\ 0 & A_{22} \end{pmatrix} \quad (17)$$

In this way, for the DTMR the value of C is equal to that calculated with the DSM and K is given by:

$$K = \frac{D_{ij}^* H_{ij}^* + 2C\bar{\Delta}^2 H_{ij}^* M_{ij}}{H_{ij}^* H_{ij}^*} \quad (18)$$

All the four dynamic models previously described are available in the numerical code employed in this study. However, for the present simulations only the DSM (Germano, *et al.* 1991), the DTM (Salvetti and Banerjee 1995) and the DTMR (Morinishi and Vasilyev 2001) are used. For all models, a local clipping has been used wherever the global viscosity, i.e., the sum of the dynamically computed SGS viscosity and the molecular one, becomes negative; in such cases, the global viscosity is set to zero, in order to avoid numerical instabilities.

For our computations, the governing equations are transformed into a general curvilinear coordinate system and discretized on a non-staggered and co-located grid using a finite volume approach (this technique is proposed in Zang, *et al.* 1994 and Zang and Street 1995). A fractional step method is employed and, to obtain the pressure field, the relevant Poisson equation is solved using a multigrid method. Time marching is semi-implicit and the formal accuracy is second order in both space and time. The details of the numerical method can be found in Zang, *et al.* (1994) and Zang and Street (1995). This numerical approach has been extensively validated (Zang, *et al.* 1994) and has been successfully used, with dynamic mixed SGS models, in previous LES of different types of flows (Zang, *et al.* 1994, Salvetti, *et al.* 1997, Salvetti, *et al.* 2001).

3. Simulation parameters and boundary conditions

For all simulations an O-type mono-bloc structured grid has been used.

No-slip conditions are employed on the cylinder surface; at the outflow of the computational domain, in the radial direction, radiative conditions are imposed in the following form:

$$\frac{\partial u_i}{\partial t} + c \frac{\partial u_i}{\partial r} = 0 \quad (19)$$

Eq. (19) is discretized in the same manner as the convective terms in the Navier-Stokes equations and c is a constant, which must be specified a priori; we set it equal to 0.6, as in Salvetti and Beux (2000). This type of boundary conditions allows the vortices to exit the domain without spurious reflection and, therefore, computational domains of reasonable dimensions in the radial direction may be used (see Salvetti and Beux 2000). At the inflow, free-stream constant conditions are imposed. Finally, periodic boundary conditions are used in the spanwise direction, in order to simulate a body of infinite length. Periodical conditions are the usual practice in numerical simulation to investigate bodies of infinite length. We have carried out a study on the sensitivity to

Table 1 Parameters of the simulations

Case	D_e/D	L_z/D	N_θ	N_r	N_z	D_r/D	N_r^1
I	20	3	128	54	8	1.145	16
II	20	3	128	54	16	1.145	16
III	20	3	128	54	32	1.145	16
IV	20	3	128	128	32	1.145	32

the spanwise dimension of the computational domain (not shown here for sake of brevity) to have indications on the minimum L_z needed to have an acceptable resolution of 3D phenomena. The values of the main flow parameters obtained with $L_z=3D$ and $L_z=6D$ were practically the same, whereas with $L_z=1.5D$ three-dimensional effects were clearly underestimated. This result is consistent with other LES studies in the literature which employ a domain spanwise length of approximately $3D$ (see, for instance, Kravchenko and Moin, 2000, Jordan and Ragab, 1998, Breuer, 1998, Franke and Frank 2002). Then we decided to carry out all other simulations by fixing $L_z=3D$.

In the spanwise direction, the dimension of the computational domain is in all cases $D_e=20D$, chosen on the basis of a previous study (Salveti and Beux 2000).

In the azimuthal and spanwise directions the grid spacing is uniform, while in the radial direction a circular refined zone is present around the cylinder to provide an adequate resolution of the boundary layer. Inside this zone (of diameter D_r) the grid spacing Δr is uniform, while outside it increases with r with a geometrical progression.

Table 1 displays the main geometrical parameters of the simulations. In particular, N_θ , N_r and N_z indicate the number of grid points respectively in the azimuthal, radial and spanwise directions and N_r^1 is the number of points in the radial direction inside the refined zone. Case I corresponds to a very coarse grid resolution, already used in Salvetti and Beux (2000). We decided here to investigate the sensitivity to grid refinement in the spanwise direction, since that of Case I appears insufficient to describe 3D features. Indeed, if we follow the rule adopted in Kravchenko and Moin (2000), the wavelength of the spanwise structures can be estimated in the near wake as: $\lambda_z/D \approx 25Re_D^{-0.5}$. This gives in our simulations $\lambda_z/D \approx 0.18$, while the grid space in the spanwise direction for case I is $\Delta z=0.375D$. Thus, the grid points in the spanwise direction are progressively doubled in cases I-III (i.e., $\Delta z=0.1875D$ in case II and $\Delta z=0.09375D$ in case III).

The effect of grid refinement in the radial direction is also investigated. Indeed, it has been found *a posteriori* that for cases I-III only approximately 2-3 grid cells are located inside the shear-layers detaching from the cylinders. Thus, in case IV, the grid points in the radial direction are doubled inside the refined zone while in the external zone are increased of the 250% in order to improve the homogeneity of the grid; in the spanwise direction the same N_z as in case III is maintained. The comparison of case IV with case III thus shows the effect of grid refinement in the radial direction.

All the simulations in Table 1 are carried out with the dynamic (DSM; Germano, *et al.* 1991) and dynamic two parameter (DTM; Salvetti and Banerjee 1995) subgrid scale models, while in case IV the DTMR (Morinishi and Vasilyev 2001) is also used.

As mentioned in the Introduction, the experimental data used for comparison are those reported in Yokuda and Ramaprian (1990), obtained in an open-circuit blower-type wind tunnel at the same

Reynolds number as in the simulations. These experiments are characterized by a blockage factor of 0.13, a cylinder aspect ratio of 8.33 and a free-stream turbulence level equal to 0.7%. These experiments have been selected among others carried out at similar Reynolds numbers and reported in the literature because of the very low level of free-stream turbulence. Indeed, it has been shown (see, for instance, Basu 1986) that the pressure distribution at the cylinder surface, in the considered regime, is very sensitive to this parameter. In large-eddy simulation is difficult to correctly reproduce the turbulent character of the free-stream flow, since in general no experimental data are available for the free-stream velocity fluctuations. Thus, as mentioned previously, a free-stream velocity constant in time is imposed and, thus, our results are more consistent with those of experiments characterized by very low free-stream turbulence intensity.

4. Effects of grid refinement

The most significant quantities for engineering applications obtained in the different simulations are summarized in Table 2. All quantities are averaged in time and in the spanwise direction ($\langle \cdot \rangle$); $\langle C_d \rangle$ is the drag coefficient, $\langle C_{pb} \rangle$ is the pressure coefficient at $\theta=180^\circ$, where θ is the azimuthal angle ($\theta=0$ at the stagnation point), and $\langle C_p^m \rangle$ and $\langle C_p^M \rangle$ are respectively the minimum (before separation) and the maximum value (after separation) of the pressure coefficient, occurring at azimuthal angles θ_m and θ_M . Finally, L_r/D is the length of the mean recirculation bubble and C_{Lrms} is the r.m.s. of the time variation of the lift coefficient. Experimental values (Yokuda and Ramaprian, 1990) are also reported in Table 2; C_{Lrms} is the one given in Basu (1985).

4.1. Grid refinement in the spanwise direction

Once the spanwise dimension of the domain has been fixed on the basis of the previous considerations, a study of the effects of the grid spacing Δz has been carried out. Referring to Table 1, we now consider cases I, II and III. We do not report the results relative to case III with DSM because the simulation got numerically unstable, due to the well known stability problems of the DSM, especially with highly inhomogeneous grids. Indeed, in case I $\Delta r_{\max}/\Delta z=2.5$ and $r_{\max}\Delta\theta/\Delta z=2.6$, in case II $\Delta r_{\max}/\Delta z=5$ and $r_{\max}\Delta\theta/\Delta z=5.2$, while in case III $\Delta r_{\max}/\Delta z=10$ and $r_{\max}\Delta\theta/\Delta z=10.4$.

An opposite behavior with increasing spanwise grid resolution is observed for the DSM and the

Table 2 Main flow parameters

Case	SGS	$\langle C_d \rangle$	$\langle C_{pb} \rangle$	$\langle C_p^m \rangle$	θ_m	$\langle C_p^M \rangle$	θ_M	L_r/D	C_{Lrms}
Exp.		1.1	-1.03	-1.17	68	-0.97	89	–	0.4±0.6
I	DSM	1.19	-1.15	-1.3	71	-0.916	115	0.70	0.61
I	DTM	1.28	-1.17	-1.21	68	-0.87	90	0.70	0.45
II	DSM	1.27	-1.38	-1.27	71	-0.91	91	0.55	0.65
II	DTM	1.15	-1.1	-1.14	68	-0.79	86	0.75	0.4
III	DTM	0.94	-0.83	-1.03	68	-0.66	87	1.4	0.17
IV	DSM	0.98	-0.96	-1.11	74	-0.90	128	0.86	0.38
IV	DTM	1.17	-1.12	-1.01	71	-0.93	85	0.77	0.51
IV	DTMR	1.02	-0.99	-1.12	74	-0.91	122	0.77	0.46

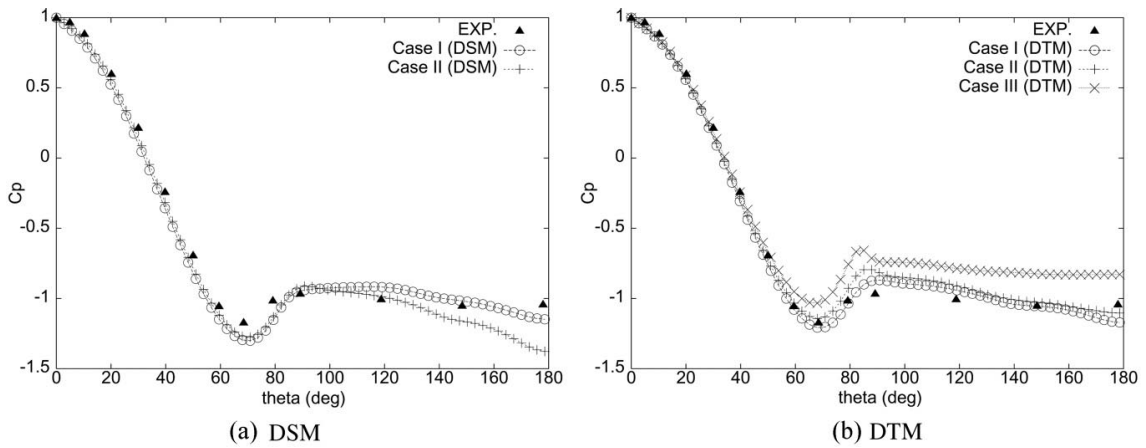


Fig. 1 Sensitivity to grid refinement in the spanwise direction; pressure coefficient versus azimuthal angle

DTM. Surprisingly, the results of the simulations carried out with the DSM become closer to those typical of 2D simulations as N_z increases. Indeed, the r.m.s. of the time variation of C_L augments and is always larger than typical values of 3D vortex shedding. Furthermore, also the drag coefficient increases with N_z and is always higher than the experimental value. In particular, discrepancies are mainly observed in the wall pressure coefficient distribution in the separated part of the flow (Fig. 1(a)). In this zone, the experimental values have a nearly constant trend, whereas the numerical curves decrease and the slope becomes steeper with increasing N_z . This behavior is also typical of 2D simulations, characterized by vortices forming closer to the cylinder surface than in 3D case and, thus, by a non-uniform induction over the cylinder rear part (see also section 5.2). Consistently, the recirculation bubble length reduces with N_z ; in particular, the value obtained in case II is clearly too low since it is typical of Reynolds numbers an order of magnitude larger. Note, for instance, that the recirculation bubble length at $Re_D = 3.9 \times 10^3$ is $L_r = 1.1D \div 1.4D$ (Kravchenko and Moin 2000) and at $Re_D = 1.4 \times 10^5$ is equal to $0.5D$ (Cantwell and Coles 1983).

An opposite trend is observed with the DTM and, as expected, 3D effects become more important as N_z is increased. However, the agreement with the experimental data is not improved, as clearly shown in Fig. 1(b). In the most refined case, for instance, the behavior of the pressure coefficient in the separated part of the flow is qualitatively correct (almost constant) but the values are significantly higher than the experimental ones and this leads to an underestimate of the drag coefficient. In this case, the r.m.s. of C_L is also noticeably underestimated while the recirculation bubble is too long; this suggests that, in the simulations with the DTM, 3D effects tend to become excessive as N_z is increased.

Summarizing, with both SGS models, the grid refinement in the spanwise direction yields a deterioration of the results. This may be due to the fact that, since the grid spacing in the other directions is kept constant, the grid becomes progressively more inhomogeneous (see Sec. 3).

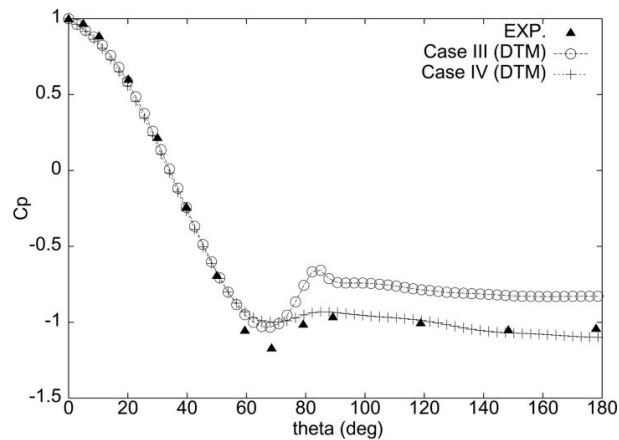


Fig. 2 Pressure coefficient versus azimuthal angle; effect of radial grid refinement

4.2. Grid refinement in the radial direction

Starting from the previous results, a grid refinement in the radial direction has also been carried out as explained in Sec. 3, with the maximum resolution in z among those previously considered (case IV in Tab. 1). Thus, we now compare cases III and IV for the DTM. The effect of this refinement is significant and the agreement with the experimental values is globally improved. In particular, in case IV the pressure coefficient fits well the experimental values in all the separated part of the flow (Fig. 2) and this leads to a good prediction of the drag coefficient. Moreover, the values of C_{Lrms} and L_r/D are now in the range of those typical of spanwise infinite cylinders at the considered Reynolds number. Nevertheless the pressure coefficient is overestimated in the expansion zone just before separation ($\theta=60^\circ-70^\circ$). The reasons of this behavior may be manifold and will be discussed in the next section.

Although grid independence and complete agreement with experiments have not been reached, in our opinion, this resolution is adequate to study the effects of SGS modeling. This analysis may give indications of the capabilities of the different models in the perspective of simulations at higher Reynolds numbers and, hence, with a limited resolution. Moreover, it is useful to understand whether it could be worth devising new SGS parameterization to obtain better predictions with reasonable grid resolution.

5. Effects of SGS modeling

Let us analyze now the effects of SGS modeling for the most refined grid (case IV).

Fig. 3 shows the C_p distribution at the cylinder for the DSM, DTM and DTMR respectively. The behavior obtained with the DSM and the DTMR is very similar; both models overestimate the C_p in the separated wake while the best agreement in this region is given by the DTM. Consequently, the DTM gives also the best prediction of the drag coefficient (see Table 2). However, as also discussed in the previous section, significant discrepancies with experimental data are observed for the DTM in the expansion zone just before separation ($\theta=60^\circ-70^\circ$), while a better agreement is obtained with the other SGS models. These differences are related to the fact that, with the DTM, the boundary

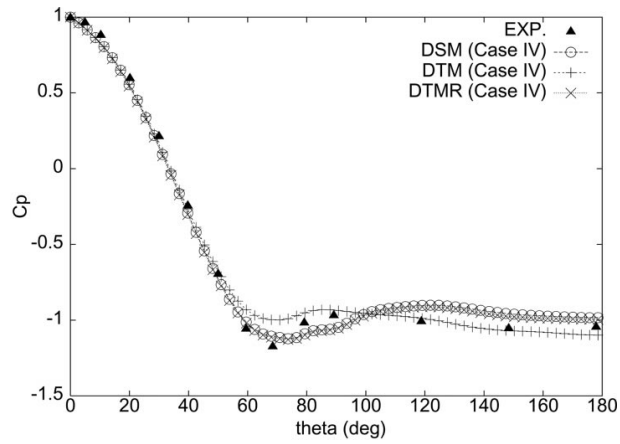


Fig. 3 Pressure coefficient versus azimuthal angle; sensitivity to SGS modeling

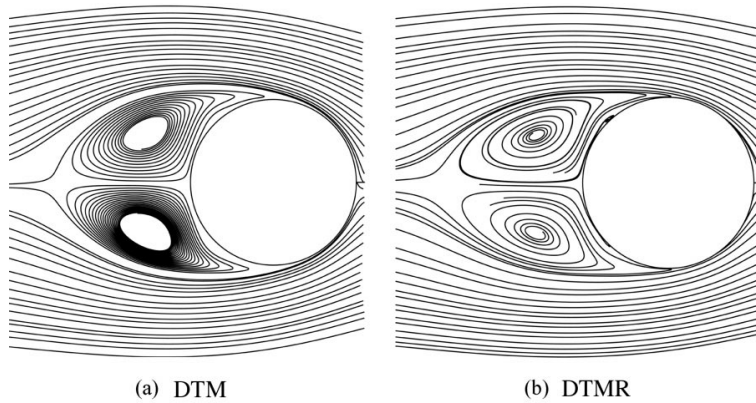


Fig. 4 Streamlines of the mean velocity field

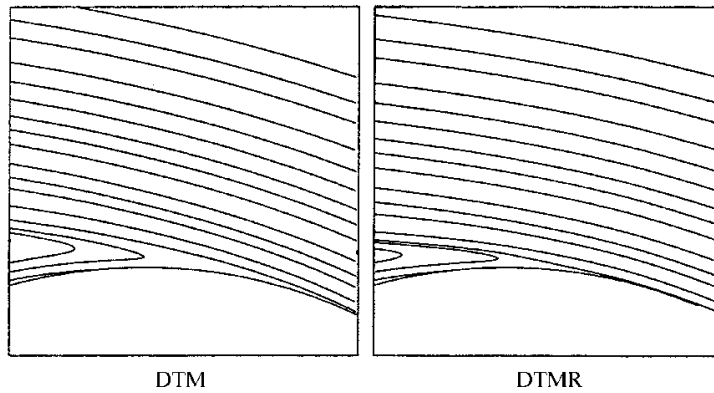


Fig. 5 Streamlines of the mean velocity field: zoom of the separation region

layer thickness just before separation is larger than with the other models and this reduces the curvature in the separation zone. The streamlines detaching from the cylinder surface are, thus,

more tilted with respect to the streamwise direction, as shown, for instance, by the streamlines of the mean velocity field in Figs. 4 and 5. The behavior of the models near the surface of the cylinder might be correlated with the importance of the Smagorinsky part in each model. The value of the parameter C is computed in the same for DSM and DTMR and those models show a better agreement with experimental value than DTM before the separation of the boundary layer, i.e., the modification proposed in Morinishi and Vasilyev (2001) seems to really improve the behavior near solid walls.

Conversely, as previously discussed, after separation the agreement with experimental values of DSM and DTMR deteriorates and DTM shows a better behavior. Thus, the modification proposed in Morinishi and Vasilyev (2001) seems to do a good job only in the attached boundary layer and this suggests that could be worth using the approximation described in Morinishi and Vasilyev (2001) only when the condition number of the matrix A is really large.

By analyzing in more detail the near wake structure obtained with the different SGS models, it appears that the different predictions given by DTM and DTMR (e.g., of the drag coefficient and of the cylinder pressure distribution) are mainly due to the different dimension and intensity of the vortices detaching from the cylinder. Indeed, with the DTM these vortices are larger and more intense than with the DTMR; consequently, as previously discussed, the near wake is thicker and the base pressure is lower. Note that the location of the vortices is the same for both models (see Fig. 4) and this confirms that the different wake width is indeed due to the different vortex intensity. With the DSM, the near wake is similar to that obtained with the DTMR, with a slightly lower transversal width. As expected from these considerations, also the shedding frequency varies with the SGS modeling. The Strouhal number, i.e., the shedding frequency adimensionalized with the cylinder diameter and the free-stream velocity, has been evaluated from the Fourier spectrum of the time variation of the C_L coefficient; values of 0.19, 0.2 and 0.21 have been obtained with the DTM, the DTMR and the DSM respectively. In Yokuda and Ramaprian (1990) a Strouhal number of 0.21 is deduced from the spectra of pressure and skin friction at different locations on the cylinder surface. However, this value is in contrast with those found in other experiments reported in the literature (see, for instance, Fey, *et al.* 1998). Following the formula proposed in Fey, *et al.* (1998), which interpolates several experimental data, a Strouhal number of 0.193 is obtained in our case.

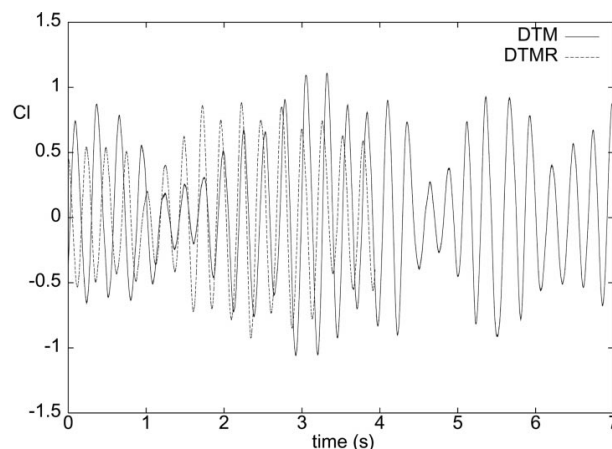


Fig. 6 Time evolution of C_L for the DTM and the DTMR

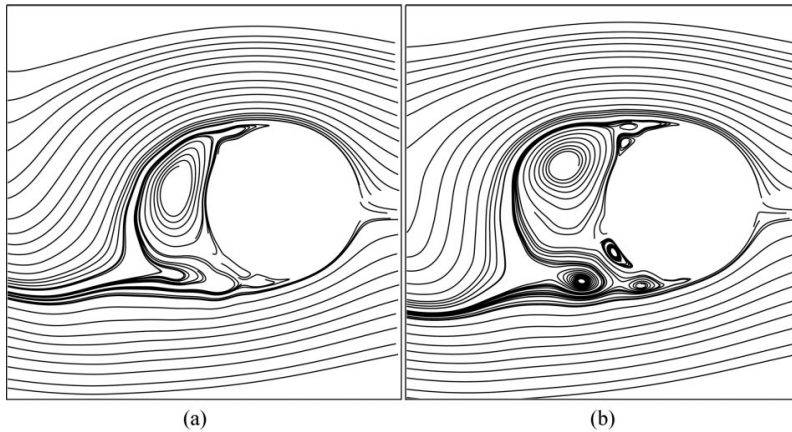


Fig. 7 Instantaneous streamlines, averaged in the spanwise direction, for the DTM. (a) Field corresponding to a high amplitude peak of the C_L (b) field corresponding to a low amplitude peak of the C_L

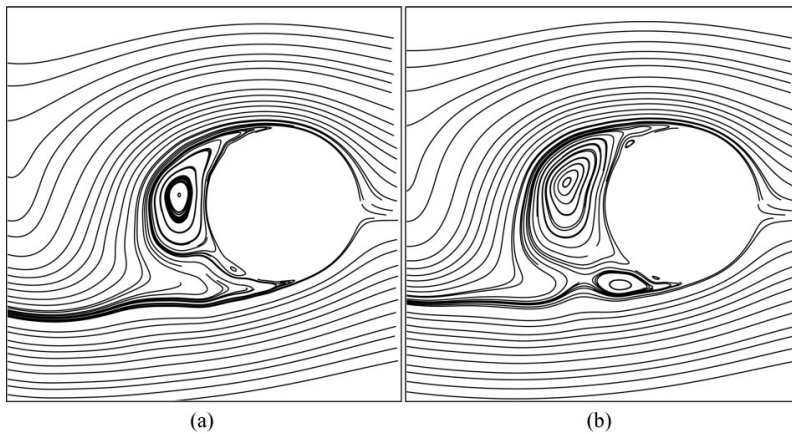


Fig. 8 Instantaneous streamlines, averaged in the spanwise direction, for the DTMR. (a) Field corresponding to a high amplitude peak of the C_L (b) field corresponding to a low amplitude peak of the C_L

The comparison of our results with this latter value confirms the considerations made when discussing the pressure distribution at the cylinder and the drag coefficient, i.e., that the DTM seems to give a better prediction of the near wake structure.

In previous experimental studies of the flow around high-aspect ratio circular cylinders (see, for instance, Cantwell and Coles 1983) low-frequency modulations of the time history of lift have been observed, and significant variations of drag correspond to these modulations; in particular, higher drag comes with higher lift amplitude. Similar behavior has been also found in large-eddy (Breuer 1998) and detached-eddy (Travin, *et al.* 1999) simulations. Our simulations with both DTM and DTMR show low-frequency amplitude modulations of C_L (Fig. 6), while they are not present with the DSM (not shown here for sake of brevity).

Looking at the instantaneous velocity fields averaged in the spanwise direction (Figs. 7 and 8), it

Table 3 Main flow parameters for the DTM, averaged on time intervals corresponding to different C_{Lrms} values

	$\langle C_D \rangle$	$\langle C_{PB} \rangle$	θ_{min}	$\langle C_{Pmin} \rangle$	C_{Lrms}	L_R/D	St
Exp.	1.1	-1.03	68.5	-1.17	0.4±0.6		
Mean	1.17	-1.12	71	-1.01	0.51	0.77	0.189
High ampl.	1.27	-1.33	71	-1.1	0.71	0.59	0.186
Low ampl.	1.02	-0.87	68	-0.88	0.23	1.18	0.192

Table 4 Main flow parameters for the DTMR, averaged on time intervals corresponding to different C_{Lrms} values

	$\langle C_D \rangle$	$\langle C_{PB} \rangle$	θ_{min}	$\langle C_{Pmin} \rangle$	C_{Lrms}	L_R/D	St
Exp.	1.1	-1.03	68.5	-1.17	0.4±0.6		
Mean	1.02	-0.99	73.7	-1.12	0.46	0.77	0.197
High ampl.	1.09	-1.11	73.7	-1.18	0.57	0.63	0.192
Low ampl.	0.93	-0.8	73.7	-1.03	0.27	0.87	0.201

can be seen that the low-frequency amplitude variations correspond to situations in which the spanwise averaged vortical structures detach from the cylinder at larger or lower distance; high amplitude C_L oscillations correspond to situations in which vortices form closer to the cylinder surface. Consequently, significantly different values of the main flow parameters characterize time intervals corresponding to high or low amplitude C_L oscillations. This can be seen, for instance, in Tables 3 and 4, which show, for DTM and DTMR respectively, the values of the global parameters obtained by averaging over the whole simulation time, and those computed only on intervals corresponding to low and high C_L amplitude oscillations.

Fig. 9 reports the corresponding C_P distributions. As expected, significant variation of the C_P

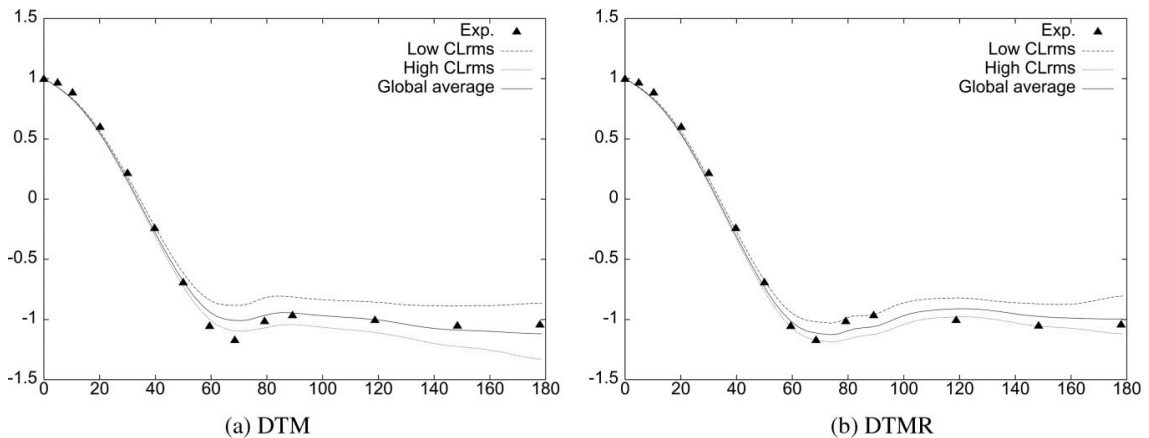


Fig. 9 Pressure coefficient versus azimuthal angle averaged on time intervals corresponding to various amplitudes of the time variation of C_L

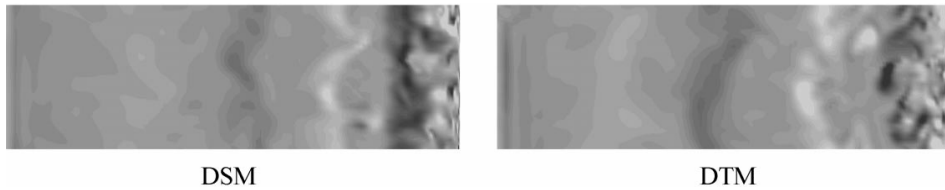


Fig. 10 Isocontours of the instantaneous spanwise vorticity component for a vertical section in the middle of the wake; the cylinder surface is on the right side of each figure. The vorticity is adimensionalized with D and U_∞ and isovalues range from -9 (black) to 5 (white).

distribution correspond to the previously described differences in the wake structures and they are more pronounced for DTM. For both SGS models, these variations start to be appreciable in the expansion zone before separation and become stronger as the azimuthal angle increases. Note that, in the time interval corresponding to high C_{Lrms} , and thus when vortices form closer to the cylinder, the C_p in the separated wake is no more constant, due to the nonuniform vortex induction.

From a technical view point, it is worth remarking that each amplitude modulation interval contains 8-12 vortex shedding cycles. Thus, it could be dangerous to compute mean quantities over only few shedding cycles, as pointed out also in Breuer (1998), Travin, *et al.* (1999), Franke and Frank (2002).

As far as the effect of SGS modeling is concerned, the low-frequency modulations and the related phenomena are slightly more pronounced with the DTM than the DTMR, while, as previously mentioned, they are absent when using the DSM. Since they are probably connected with the 3D character of the wake, one may argue that the scale similarity term in mixed models is effective in introducing 3D features in the flow, as could be anticipated since it gives an anisotropic contribution to the SGS stress tensor. The more pronounced 3D character of the near wake obtained with the DTM compared with that given by the DSM can also be seen, for instance, from Fig. 10, which shows the instantaneous isocontours of the spanwise vorticity obtained in the vertical section in the middle of the wake. The considered instantaneous fields correspond to maxima in the C_L time history.

In the instantaneous velocity fields (Figs. 7 and 8) differences between the DTM and the DTMR can be observed also in secondary separations; in particular, with the DTM, more small recirculating regions are present just downstream the boundary layer separation.

6. Conclusions

Large-eddy simulations of the flow around a circular cylinder at $Re_D=2 \times 10^4$ have been presented.

Starting from a grid resolution much coarser than those generally used in LES in the literature, the effects of grid refinement in the spanwise direction have been studied systematically, for the dynamic eddy-viscosity model and a two-parameter mixed dynamic model. Two opposite behaviors have been observed. Unexpectedly, with the DSM, the spanwise refinement yields results which are closer to those typical of 2D simulations, while with the DTM, 3D effects become, as anticipated, more important. However, for both SGS models, the agreement with the experimental data is

deteriorated with the spanwise refinement and this is probably due to the fact that the grid becomes progressively more inhomogeneous.

On the basis of this analysis, a further refinement in the radial direction has been carried out and this has led, as expected, to a significant improvement of the accuracy of the results. Although grid independence and complete agreement with experiments were not reached, in our opinion, the finest considered resolution was adequate to study the effects of SGS modeling. This analysis may give indications of the capabilities of the different models in the perspective of simulations at higher Reynolds numbers and, hence, with a limited resolution. Moreover, it helps understand whether it could be worth devising new SGS parameterization to obtain better prediction with reasonable grid resolution. Thus, the effects of the SGS modeling were studied for this *fine* grid. A modified version of the DTM (DTMR) was also considered.

In the expansion part on the cylinder ($\theta < 70^\circ$) the DTM has been found to give too large a boundary layer thickness and this may be due to near wall problems of the DTM highlighted in Morinishi and Vasilyev (2001). The modification in the computation of the model parameters in the DTMR effectively yields results that are closer to those obtained with the dynamic eddy-viscosity model and in better agreement with the experiments.

Conversely, in the separation zone and in the wake the DTM is found to give more accurate results than the other models. The differences in model predictions appear to be mainly related to different dimension and intensity of the vortices detaching from the cylinder.

Furthermore, with the grid resolution considered here, the DSM appears to be unable to correctly capture the low-frequency modulations of the aerodynamic lift, which are conversely present in simulations with both the DTM and the DTMR. Since these modulations are probably due to the 3D character of the wake, it seems that the scale similarity term in mixed models is the main responsible of the introduction of 3D features in the flow. By analyzing the instantaneous fields obtained with the DTM and the DTMR, it has been shown that the low-frequency amplitude variations correspond to situations in which the spanwise averaged vortical structures detach from the cylinder at larger or lower distance. As a consequence, significantly different values of the main flow parameters characterize time intervals corresponding to high or low amplitude C_L oscillations. This confirms that it may be dangerous to compute averaged quantities on a few shedding cycles, as already pointed out in Breuer (1998), Travin, *et al.* (1999), Franke and Frank, (2002).

Summarizing, also on the finest considered grid, the effects of SGS modeling are significant and mixed models appear to be more suitable for large-eddy simulations of this type of flows than eddy-viscosity ones.

The present study also suggests that the accuracy of LES results could be improved, not only by further refining the computational grid, but also by deriving a dynamic SGS mixed model that combines the positive features of DTM in the separated regions and those of DTMR in the attached boundary layer.

References

- Bardina, J., Ferziger, J.-H. and Reynolds, W.-C. (1984), "Improved turbulence models based on large eddy simulation of homogeneous incompressible flows", Technical Report TF-19, Department of Mechanical Engineering, Stanford University.
- Basu, R.-I. (1985), "Aerodynamic forces on structures of circular cross-section. Part I: Model-scale data obtained

- under two-dimensional condition in low-turbulence streams”, *J. Wind Eng. Ind. Aerodyn.*, **21**, 273-294.
- Basu, R.-I. (1986), “Aerodynamic forces on structures of circular cross-section. Part 2: The influence of turbulence and three-dimensional effects”, *J. Wind Eng. Ind. Aerodyn.*, **24**, 33-59.
- Breuer, M. (1998), “Large eddy simulation of the sub-critical flow past a circular cylinder: numerical and modeling aspects”, *Int. J. Numer. Meth. Fluids*, **28**, 1281-1302.
- Breuer, M. (2000), “A challenging test case for large eddy simulation: high Reynolds number circular cylinder flow”, *Int. J. Heat Fluid Flow*, **21**, 648-654.
- Cantwell, B. and Coles, D. (1983), “An experimental study of entrainment and transport in the turbulent near wake of a circular cylinder”, *J. Fluid Mech.*, **136**, 321-374.
- Fey, U., König, M. and Eckelmann, H. (1998), “A new Strouhal-Reynolds-number relationship for the circular cylinder in the range $47 < Re < 2 \times 10^5$ ”, *Phys. Fluids*, **10**, 1547-1549.
- Franke, J. and Frank, W. (2002), “Large eddy simulation of the flow past a circular cylinder at $Re_D=3900$ ”, *J. Wind Eng. Ind. Aerodyn.*, **90**, 1191-1206.
- Fröhlich, J., Rodi, W., Kessler, P., Parpais, S., Bertoglio, J. and Laurence, D. (1998), “Large eddy simulation of flow around circular cylinders on structured and unstructured grids”, In Hirschel, E.-H., editor, *Notes on numerical fluid mechanics*. Vieweg.
- Germano, M., Piomelli, U., Moin, P. and Cabot, W.-H. (1991), “A dynamic subgrid-scale eddy-viscosity model”, *Phys. Fluids A*, **3**, 1760-1765.
- Jordan, S.-A. and Ragab, S.-A. (1998), “A large-eddy simulation of the near wake of a circular cylinder”, *J. Fluids Eng.*, **120**, 243-252.
- Kravchenko, A.-G. and Moin, P. (2000), “Numerical studies of flow over a circular cylinder at $Re_D=3900$ ”, *Phys. Fluids*, **12**(2), 403-417.
- Lübcke, H., Schmidt, S., Rung, T. and Thiele, F. (2001), “Comparison of LES and RANS in bluff-body flows”, *J. Wind Eng. Ind. Aerodyn.*, **89**, 1471-1485.
- Ma, X., Karamanos, C.-S. and Karniadakis, G.-E. (2000), “Dynamics and low-dimensionality of a turbulent near wake”, *J. Fluid Mech.*, **410**, 29-65.
- Meneveau, C. and Katz, J. (2000), “Scale-invariance and turbulence models for large-eddy simulation”, *Annu. Rev. Fluid Mech.*, **32**, 1-32.
- Mittal, R. and Moin, R. (1997), “Suitability of upwind-biased finite difference schemes for large-eddy simulation of turbulent flows”, *AIAA J.*, **35**(8), 1415-1417.
- Morinishi, Y. and Vasilyev, O.-V. (2001), “A recommended modification to the dynamic two-parameter subgrid scale model for large eddy simulation of wall bounded turbulent flow”, *Phys. Fluids*, **13**, 3400-3410.
- Salvetti, M.-V., Zang, Y., Street, R.-L. and Banerjee, S. (1997), “Large-eddy simulation of free-surface decaying turbulence with dynamic subgrid-scale models”, *Phys. Fluids*, **9**, 2405-2419.
- Salvetti, M.-V. and Banerjee, S. (1995), “A priori tests of a new dynamic subgrid-scale model for finite-difference large-eddy simulations”, *Phys. Fluids*, **7**, 2831-2847.
- Salvetti, M.-V. and Beux, F. (2000), “Large-eddy simulation of the flow around a circular cylinder with dynamic subgrid-scale models”, In *Atti del 6° Convegno Nazionale di Ingegneria del Vento IN-VENTO-2000*, Pages 293-300, Gune, 18-21, June.
- Salvetti, M.-V., Damiani, R. and Beux, F. (2001), “3D coarse large-eddy simulations of the flow above two-dimensional sinusoidal waves”, *Int. J. Num. Meth. Fluids*, **35**, 617-642.
- Smagorinsky, J. (1963), “General circulation experiments with the primitive equations. i. the basic experiment”, *Mon. Weather Rev.*, **91**, 99-164.
- Travin, A., Shur, M., Strelets, M. and Spalart, P. R. (1999), “Detached-eddy simulation past a circular cylinder”, *Flow, Turb. Comb.*, **63**, 293-313.
- Yokuda, S. and Ramaprian, R.-R. (1990), “The dynamics of flow around a cylinder at subcritical Reynolds number”, *Phys. Fluids A*, **2**(5), 784-791.
- Zang, Y. and Street, R.-L. (1995), “A composite multigrid method for calculating unsteady incompressible flows in geometrically complex domains”, *Int. J. Num. Meth. in Fluids*, **20**, 341-361.
- Zang, Y., Street, R.-L. and Koseff, J.-R. (1993), “A dynamic mixed subgrid-scale model and its application to turbulent recirculating flows”, *Phys. Fluids A*, **5**, 3186-3196.
- Zang, Y., Street, R.-L. and Koseff, J.-R. (1994), “A non-staggered grid, fractional step method for time-

dependent incompressible Navier-Stokes equations in general curvilinear coordinate systems”, *J. Comput. Phys.*, **114**, 18-33.